

# Temperature feedback-controlled photothermal treatment with diffusing applicator: theoretical and experimental evaluations

Trung Hau Nguyen,<sup>1,4</sup> Suhyun Park,<sup>2,4</sup> Kyu Kyu Hlaing,<sup>1</sup> and Hyun Wook Kang<sup>1,3,\*</sup>

<sup>1</sup>Interdisciplinary Program of Biomedical Mechanical & Electrical Engineering, Pukyong National University, Busan 48513, South Korea

<sup>2</sup>Samsung Advanced Institute of Technology, Samsung Electronics, Suwon 16678, South Korea

<sup>3</sup>Department of Biomedical Engineering and Center for Marine-Integrated Biomedical Technology (BK 21 Plus), Pukyong National University, Busan 48513, South Korea

<sup>4</sup>These authors equally contributed to this work

\*wkang@pukyong.ac.kr

**Abstract:** To minimize thermal injury, the current study evaluated the real-time temperature monitoring with a proportional-integrative-derivative (PID) controller during 980-nm photothermal treatment with a radially-diffusing applicator. Both simulations and experiments demonstrated comparable thermal behaviors in temperature distribution and the degree of irreversible tissue denaturation. The PID-controlled application constantly maintained the pre-determined temperature of 353 K (steady-state error = < 1 K). Due to constant energy delivery, coagulation volumes linearly increased up to  $1.04 \pm 0.02 \text{ cm}^3$  with irradiation time. Integration of temperature feedback with diffuser-assisted photothermal treatments can provide a feasible therapeutic modality to treat pancreatic tumors in an effective manner.

©2016 Optical Society of America

**OCIS codes:** (000.4430) Numerical approximation and analysis; (140.6810) Thermal effects; (170.1610) Clinical applications; (230.1980) Diffusers.

## References and links

1. B. W. Chang and M. W. Saif, "Stereotactic body radiation therapy (SBRT) in pancreatic cancer: is it ready for prime time?" *JOP* **9**(6), 676–682 (2008).
2. B. W. Stewart and C. P. Wild, *World Cancer Report 2014* (International Agency for Research on Cancer, Lyon Cedex, France, 2014).
3. S. Raimondi, P. Maisonneuve, and A. B. Lowenfels, "Epidemiology of pancreatic cancer: an overview," *Nat. Rev. Gastroenterol. Hepatol.* **6**(12), 699–708 (2009).
4. D. Yadav and A. B. Lowenfels, "The epidemiology of pancreatitis and pancreatic cancer," *Gastroenterology* **144**(6), 1252–1261 (2013).
5. M. Kayahara, T. Nagakawa, K. Ueno, T. Ohta, T. Takeda, and I. Miyazaki, "An evaluation of radical resection for pancreatic cancer based on the mode of recurrence as determined by autopsy and diagnostic imaging," *Cancer* **72**(7), 2118–2123 (1993).
6. D. Li, K. Xie, R. Wolff, and J. L. Abbruzzese, "Pancreatic cancer," *Lancet* **363**(9414), 1049–1057 (2004).
7. M. G. Keane, K. Bramis, S. P. Pereira, and G. K. Fusai, "Systematic review of novel ablative methods in locally advanced pancreatic cancer," *World J. Gastroenterol.* **20**(9), 2267–2278 (2014).
8. R. Girelli, I. Frigerio, R. Salvia, E. Barbi, P. Tinazzi Martini, and C. Bassi, "Feasibility and safety of radiofrequency ablation for locally advanced pancreatic cancer," *Br. J. Surg.* **97**(2), 220–225 (2010).
9. G. Carrafiello, A. M. Ierardi, F. Fontana, M. Petrillo, C. Floridi, N. Lucchina, S. Cuffari, G. Dionigi, A. Rotondo, and C. Fugazzola, "Microwave ablation of pancreatic head cancer: safety and efficacy," *J. Vasc. Interv. Radiol.* **24**(10), 1513–1520 (2013).
10. K. C. Xu, L. Z. Niu, Y. Z. Hu, W. B. He, Y. S. He, and J. S. Zuo, "Cryosurgery with combination of (125)iodine seed implantation for the treatment of locally advanced pancreatic cancer," *J. Dig. Dis.* **9**(1), 32–40 (2008).
11. M. T. Huggett, M. Jermyn, A. Gillams, S. Mosse, E. Kent, S. G. Bown, T. Hasan, B. W. Pogue, and S. P. Pereira, "Photodynamic therapy for locally advanced pancreatic cancer (vertpac study)- final clinical results," *Pancreatology* **13**(1), e2–e3 (2013).

12. R. Suzuki, A. Irisawa, and M. S. Bhutani, "Endoscopic Ultrasound-Guided Oncologic Therapy for Pancreatic Cancer," *Diagn. Ther. Endosc.* **2013**, 157581 (2013).
13. P. Saccomandi, E. Schena, M. A. Caponero, F. M. Di Matteo, M. Martino, M. Pandolfi, and S. Silvestri, "Theoretical analysis and experimental evaluation of laser-induced interstitial thermotherapy in ex vivo porcine pancreas," *IEEE Trans. Biomed. Eng.* **59**(10), 2958–2964 (2012).
14. D. Fuentes, J. T. Oden, K. R. Diller, J. D. Hazle, A. Elliott, A. Shetty, and R. J. Stafford, "Computational modeling and real-time control of patient-specific laser treatment of cancer," *Ann. Biomed. Eng.* **37**(4), 763–782 (2009).
15. T. H. Nguyen, Y. H. Rhee, J. C. Ahn, and H. W. Kang, "Circumferential irradiation for interstitial coagulation of urethral stricture," *Opt. Express* **23**(16), 20829–20840 (2015).
16. A. Vogel and V. Venugopalan, "Mechanisms of pulsed laser ablation of biological tissues," *Chem. Rev.* **103**(2), 577–644 (2003).
17. N. M. H., *Laser-tissue Interactions: Fundamentals and Applications* (Springer-Verlag, 2004).
18. M. Rieken, H. W. Kang, E. Koullick, G. R. Ruth, and A. Bachmann, "Laser vaporization of the prostate in vivo: Experience with the 150-W 980-nm diode laser in living canines," *Lasers Surg. Med.* **42**(8), 736–742 (2010).
19. M. N. Iizuka, I. A. Vitkin, M. C. Kolios, and M. D. Sherar, "The effects of dynamic optical properties during interstitial laser photocoagulation," *Phys. Med. Biol.* **45**(5), 1335–1357 (2000).
20. J. A. Burns, J. B. Kobler, J. T. Heaton, G. Lopez-Guerra, R. R. Anderson, and S. M. Zeitel, "Thermal damage during thulium laser dissection of laryngeal soft tissue is reduced with air cooling: ex vivo calf model study," *Ann. Otol. Rhinol. Laryngol.* **116**(11), 853–857 (2007).
21. E. G. Macchi, D. Tosi, G. Braschi, M. Gallati, A. Cigada, G. Busca, and E. Lewis, "Optical fiber sensors-based temperature distribution measurement in ex vivo radiofrequency ablation with submillimeter resolution," *J. Biomed. Opt.* **19**(11), 117004 (2014).
22. Y. Feng and D. Fuentes, "Model-based planning and real-time predictive control for laser-induced thermal therapy," *Int. J. Hyperthermia* **27**(8), 751–761 (2011).
23. L. M. Vesselov, W. Whittington, and L. Lilje, "Performance evaluation of cylindrical fiber optic light diffusers for biomedical applications," *Lasers Surg. Med.* **34**(4), 348–351 (2004).
24. S. C. Jiang and X. X. Zhang, "Dynamic modeling of photothermal interactions for laser-induced interstitial thermotherapy: parameter sensitivity analysis," *Lasers Med. Sci.* **20**(3-4), 122–131 (2005).
25. A. Ishimaru, "Diffusion of light in turbid material," *Appl. Opt.* **28**(12), 2210–2215 (1989).
26. G. Yoon, A. J. Welch, M. Motamedi, and M. Gemert, "Development and application of three-dimensional light distribution model for laser irradiated tissue," *Quantum Electronics, IEEE Journal of* **23**(10), 1721–1733 (1987).
27. B. C. Wilson and G. Adam, "A Monte Carlo model for the absorption and flux distributions of light in tissue," *Med. Phys.* **10**(6), 824–830 (1983).
28. A. Kiam Heong, G. Chong, and L. Yun, "PID control system analysis, design, and technology," *IEEE Trans. Contr. Syst. Technol.* **13**(4), 559–576 (2005).
29. K. Ahrar, A. Gowda, S. Javadi, A. Borne, M. Fox, R. McNichols, J. U. Ahrar, C. Stephens, and R. J. Stafford, "Preclinical assessment of a 980-nm diode laser ablation system in a large animal tumor model," *J. Vasc. Interv. Radiol.* **21**(4), 555–561 (2010).
30. Y. Mohammed and J. F. Verhey, "A finite element method model to simulate laser interstitial thermo therapy in anatomical inhomogeneous regions," *Biomed. Eng. Online* **4**(1), 2 (2005).
31. J. P. Ritz, A. Roggan, C. Isbert, G. Müller, H. J. Bühr, and C. T. Germer, "Optical properties of native and coagulated porcine liver tissue between 400 and 2400 nm," *Lasers Surg. Med.* **29**(3), 205–212 (2001).
32. S. L. Jacques and S. A. Prahl, "Modeling optical and thermal distributions in tissue during laser irradiation," *Lasers Surg. Med.* **6**(6), 494–503 (1987).
33. A. H. Dachman, P. M. MacEneaney, A. Adedipe, M. Carlin, and L. P. Schumm, "Tumor size on computed tomography scans: is one measurement enough?" *Cancer* **91**(3), 555–560 (2001).
34. A. J. Welch and M. J. C. van Gemert, *Optical-thermal Response of Laser-Irradiated Tissue* (Plenum Press, 1995).

---

## 1. Introduction

Due to poor prognosis and short survival times of 4–6 months [1], pancreatic ductal adenocarcinoma (PDAC) is the seventh cause of cancer deaths worldwide [2] and the fourth in US [3]. Globally, the incidence rate of the pancreatic cancer is around 8 out of 100,000 persons [4]. More than 227,000 people die from the disease per year worldwide [3]. The symptoms include nausea, weight loss, yellow skin, and dark urine. Surgical resection can be applicable for the pancreatic tumors in size of less than 3 cm (stage I and IIA) in any direction, which solely occurs in the pancreas [5, 6]. However, for unresectable tumors, minimally invasive ablative therapies can be performed as a standard procedure in a percutaneous or endoscopic manner [7]. On account of technological advances in therapeutic and diagnostic devices, a number of thermal techniques have been evaluated to treat locally advanced or metastatic PDAC such as radiofrequency ablation (RFA), microwave ablation

(MWA), cryoablation (CA), photodynamic therapy (PDT), and high intensity focused ultrasound (HIFU) [8–12]. RFA induces necrotic tissue destruction by applying a high frequency alternating current to the tumor. However, high temperatures ( $> 90^{\circ}\text{C}$ ) often lead to excessive thermal damage to adjacent tissue structures leading to high complications and morbidity rates ( $\sim 10\%$ ) [7, 8]. MWA was intraoperatively performed with during palliative bypass surgery and still associated with minor complications such as mild pancreatitis and bleeding [7, 9]. CA was applied to freeze the tumor down to  $-160^{\circ}\text{C}$  and to create ice balls to encompass the entire mass for necrosis, but the procedures need a 5 mm safety margin from the surrounding structures. Fiber-based PDT promotes tumor ablation by generating singlet oxygen after light interaction with photosensitizer [11]. Lengthy (up to several days) irradiation can be a significant drawback, possibly resulting in skin necrosis. In addition, many new photosensitizers are still under clinical investigations [7]. Lastly, HIFU is used as a non-invasive thermal treatment on the tumors. Although successful preclinical experiences have been reported, real-time temperature compensation is limitedly available during the procedure [7, 12].

Recently, laser interstitial thermal treatment (LITT) was employed as a minimally invasive ablation method to achieve deep coagulation in pancreatic tumor [13]. Due to light guidance of optical fibers, *ex vivo* LITT studies showed the promising results on thermal treatment in terms of theoretical modeling and experimental comparison. However, the LITT treatment used a flat-cut bare fiber that merely delivered the laser light in a forward direction [13]. Thus, as the tumor often develops in the form of ellipsoid along the 15-cm long pancreas, the diverging laser light hardly obtains the uniform coagulation within the tumor volume particularly in a circumferential direction. Delivery of lower optical energy to the tissue is often associated with the lengthy procedure time up to 18 mins to thermally cover the entire target [14]. Furthermore, the beam divergence from the small fiber core (300  $\mu\text{m}$ ) can result in high concentration of optical energy at the tissue surface with inhomogeneous temperature distribution inside the tissue [13]. In order to overcome the inherent limitations of the bare optical fibers, a diffusing optical applicator was developed and evaluated for photothermal treatment of tubular tissue structures [15]. Due to uniform and radial light emissions, the diffusing tip was able to achieve circumferential coagulation in the tissue over the 1-cm length. Therefore, the application of the radially diffusing optical device can be a feasible method to treat the tubular tissues such as pancreas in an effective manner with minimal collateral injury to duodenum.

During photothermal treatment, irradiance and exposure time are critical factors to determine the degree of irreversible denaturation [16]. Particularly, long irradiation times to attain deep tissue coagulation often causes surface carbonization due to substantial thermal gradients developed within the tissue volume [17]. Moreover, severe thermal injury can adversely affect the delayed healing responses of the treated tissue, possibly leading to collagenous fibrosis [18]. Thus, the real-time monitoring of the tissue temperature can be pivotal to minimizing undesirable thermal injury and to maximizing clinical outcomes during the laser treatment. In fact, a variety of thermal monitoring methods, such as thermocouple [19], thermistor [20], optical fiber sensor [21], and magnetic resonance imaging [22], have been implemented to measure and identify the spatio-temporal developments of the temperature in the tissue. The aim of the current study was to evaluate the feasibility of thermocouple-assisted laser treatment on PCDA with radially-diffusing applicators. It was hypothesized that the real-time thermal monitoring during the irradiation could contribute to reliable generation of the treatment regions in circumferential manners. To constantly maintain the tissue surface temperature, a proportional-integrative-derivative (PID) controller in conjunction with a thermocouple was implemented during the diffuser-assisted photocoagulation. Both numerical modeling and experimental analysis were comparatively implemented to assess the development of the interstitial temperature and the degree of thermal coagulation.

## 2. Materials and methods

### 2.1. Diffusing applicator

Figure 1(a) demonstrates a microscopic image of an optically diffusing applicator prepared for the current study. A multimode 600- $\mu\text{m}$  core diameter fiber (NA = 0.48, Thorlabs Inc., Newton, New Jersey, USA) was tapered and fabricated by using a CO<sub>2</sub> laser to achieve a 10-*mm* long diffusing tip. Then, the fabricated tip was sealed with a customized glass cap (i.e., length = 14 *mm* and outer diameter = 1.4 *mm*) for mechanical protection by using epoxy. The detailed information on tip fabrication was reported in a previous study [15]. Prior to experiments, the diffusing applicator was evaluated in terms of power distribution in polar and longitudinal directions by using a goniometric measurement system that consisted of a photodiode (PD-300-3W, Ophir, Jerusalem, Israel) and a HeNe laser [23]. Figures 1(b) and 1(c) exhibit the spatial distribution of the normalized intensity for the polar and the longitudinal emissions, respectively. The polar results showed almost uniform and circumferential radiation with less than 5% deviation from the mean angular intensity (i.e.,  $0.95 \pm 0.03$  in Fig. 1(b)). The normalized polar intensities ranged from 0.92 to 1.00 (i.e. 8% difference). The longitudinal emission demonstrated an asymmetric (left-skewed) profile of the light distribution with less than 15% deviation along the applicator (i.e.,  $0.75 \pm 0.14$  in Fig. (c)). The highest intensity occurred near the proximal end of the diffuser (2.5 *mm*), and the normalized intensity almost gradually decreased along the diffusing tip toward the distal end. The variation between the highest and the lowest intensities was less than 38%. In addition, the power measurements confirmed that 5% of the input power was transmitted in a forward direction of the fiber end.

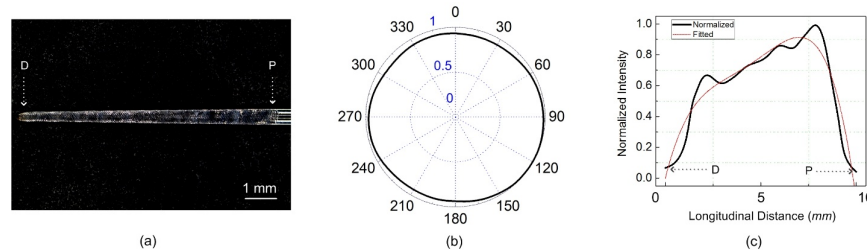


Fig. 1. Evaluations on diffusing optical applicator: (a) microscopic image, (b) polar emissions, and (c) longitudinal emissions. A red line represents the curve fitting (P = proximal and D = distal ends)

### 2.2. Numerical simulations

Numerical simulations were conducted to predict thermal responses (temperature distribution and thermal damage) of tissue during laser irradiation. Based upon physical dimensions of the fabricated diffusing applicator aforementioned, Fig. 2(a) demonstrates a simulation model of a glass-capped diffuser (i.e., length = 14 *mm*, outer diameter = 1.4 *mm*, and cap thickness = 0.2 *mm*) that was inserted into a tissue specimen of  $30 \times 30 \times 30 \text{ mm}^3$ . A 0.2-*mm* air gap existed between the diffuser and the inner wall of the glass cap. A 1-*mm* thick layer of air was also located in front of the distal end of the diffuser tip. It should be noted that the actual light was transmitted from the diffuser tip and thus, the length of the line light source was considered 11 *mm*. As a light source, a 10-*W* 980-*nm* wavelength was employed to induce photothermal response of tissue for the current study.

An integro-differential equation was used to mathematically describe the transport of light in tissue [24]. Instead of solving the complex equation, a number of analytical approximations have been proposed such as diffusion approximation [25], seven flux model [26], and Monte Carlo simulation [27]. For the current study, a simple diffusion approximation method was employed to predict light propagation in tissue by using the Beer's law [16, 17]:

$$I(d) = I_0 \cdot e^{-\mu_t \cdot d} \quad (1)$$

where  $I$  ( $W/cm^2$ ) is the fluence rate at the tissue depth of  $d$  ( $cm$ ),  $I_0$  ( $W/cm^2$ ) the irradiance at the surface, and  $\mu_t$  ( $cm^{-1}$ ) the total attenuation coefficient. The laser light absorption in the tissue results in heat accumulation and volumetric temperature rise. In turn, the deposited thermal energy can diffuse to the surrounding tissue. Thermal behaviors in the tissue can be described by using a bio-heat transfer equation (called Pennes' equation) as follows [17]:

$$\rho c \frac{\partial T}{\partial t} + \nabla(-k\nabla T) = \rho_b c_b \omega_b (T_b - T) + Q_{met} + Q_{ext} \quad (2)$$

where  $\rho$  ( $kg/m^3$ ),  $c$  ( $J/kg\cdot K$ ), and  $k$  ( $W/m\cdot K$ ) are density, specific heat, and thermal conductivity of the tissue respectively,  $T$  ( $K$ ) the local tissue temperature,  $\rho_b$  ( $kg/m^3$ ),  $c_b$  ( $J/kg\cdot K$ ), and  $k_b$  ( $W/m\cdot K$ ) the density, specific heat, and thermal conductivity of blood, respectively,  $T_b$  ( $K$ ) the temperature of arterial blood,  $Q_{met}$  ( $W/cm^3$ ) the metabolic heat source, and  $Q_{ext}$  ( $W/m^3$ ) the heat source generated by light absorption. Since all the experiments were conducted *ex vivo* for the current study, the effects of the metabolic heat source ( $Q_{met}$ ) and blood perfusion on tissue ( $\omega_b$ ) were assumed insignificant during the simulations. Table 1 presents a summary of thermal properties used in the current simulations.

**Table 1. Thermal properties of materials used in numerical simulations**

Material	$k$ ( $W/m\cdot K$ )	$\rho$ ( $kg/m^3$ )	$c$ ( $J/kg\cdot K$ )	Reference
Glass	1.3	2200	820	[15]
Air	0.0257	1.205	1005	[15]
Liver tissue	0.513	1050	3600	[15]

Then, Eq. (2) was numerically solved by using a finite-element method (v5.0, COMSOL Inc., Burlington, Massachusetts, USA). For the sake of simplification, the current model assumed that the laser intensity consisted of two directional laser powers: radial emission from the diffusing part,  $P_1$  (assuming 95% of the incident laser power) and forward emission from the fiber tip,  $P_2$  (5% of the incident laser power). For the radial direction, variations in the laser intensity were quantified by curve-fitting a spatial emission profile of the diffuser in Fig. 1(c). Since the polar intensity profile yielded an almost isotropic distribution of the light in Fig. 1(b), the longitudinal intensity was merely contingent upon the diffuser length ( $d_l$  in  $m$ ) from the proximal to the distal ends. Consequently, the normalized longitudinal intensity ( $I_0$ ) was estimated in a form of polynomial function with degree of four as follows:

$$I_0(d_l) = -2.1 \times 10^9 \cdot d_l^4 + 4.5 \times 10^7 \cdot d_l^3 - 343370 \cdot d_l^2 + 1044 \cdot d_l - 0.09 \quad (3)$$

The longitudinal intensity ( $I_l$  in  $W/m^2$ ) was assumed to be proportional to  $I_0$  by a factor of  $K$ .

$$I_l(d_l) = K \cdot I_0(d_l) \quad (4)$$

The proportional factor was then calculated from the double integral of two variables (i.e., diffuser length and polar angle) that represented the surface area of the glass-cap at the laser-tissue interface. The intervals for the diffuser length and the polar angle were from 0 to 0.01  $m$  and from 0 to  $2\pi$ , respectively. The result of the double integral in the cylindrical coordinate was equal to the radial laser power ( $P_1$  in  $W$ ) used for the current study as follows:

$$\iint K \cdot I_0(d_l) dA = P_1 \quad (5)$$

where  $dA$  is the unit area on the surface of the glass cap. Thus, the solution of Eq. (5) defined the proportional factor, which provided the values for  $I_l$  as a function of  $d_l$ . Therefore, the heat source in the radial direction was determined as follows:

$$Q_{ext} = \mu_a \cdot I_l \cdot e^{-\mu_a \cdot r} \quad (6)$$

where  $\mu_a$  ( $cm^{-1}$ ) is the absorption coefficient of laser light in tissue, and  $r$  ( $m$ ) the radial distance from the glass cap [15]. For the forward direction, the light was diverged from the fiber tip ( $NA = 0.48$ ), and the spatial beam profile was assumed to be Gaussian. Thus, the heat source depended upon both the radial and the axial distances according to the spatial emission:

$$Q_{ext} = \frac{\mu_a P_2}{2\pi\sigma^2} e^{\frac{-r}{2\sigma^2}} \cdot e^{-\mu_a \cdot z} \quad (7)$$

where  $\sigma$  is the deviation of Gaussian distribution of the laser beam (i.e.,  $100 \mu m$  resulting from 99% of the output laser power at the fiber surface with a radius of  $300 \mu m$ ) and  $z$  ( $m$ ) the axial depth in tissue. The initial tissue temperature was set to  $293 K$ , and the external surface of the tissue was insulated (i.e.,  $\vec{n} \cdot \vec{k} \cdot \nabla T = 0$ , where  $\vec{n}$  is the direction of the heat flux).

In order to evaluate the effect of a PID-controller on tissue temperature, three different modes were compared during laser irradiation with  $10-W$   $980 nm$ : continuous-wave (CW), pulsed, and PID-controlled. For CW application, the laser light was continuously delivered for  $30 s$  to the tissue through a diffusing applicator. In the pulsed mode, the light was modulated at a 50% duty cycle (i.e., pulse duration =  $0.25 s$  operating at  $2 Hz$ ). Lastly, the PID-controlled mode was implemented to limit the maximum temperature at the cap-tissue interface to  $353 K$ , which was the upper limit temperature for irreversible thermal denaturation [16]. Thus, the establishment of the pre-determined temperature prevented any overshooting in temperature elevations from the transient responses of the PID controller during the irradiation. Based upon temperature feedback, the laser power was thus continuously modulated. An algorithm of the PID controller is based on the error signals between the desired set-point and process variables, which attempts to minimize the errors by changing the output signals. The general form of the PID algorithm is a summation of proportional, integral, and derivative terms as follows [28]:

$$u(t) = K_p e(t) + K_i \int_0^t e(\tau) d\tau + K_d \frac{d}{dt} e(t) \quad (8)$$

where  $u(t)$  is control signal,  $e(t)$  error (i.e., difference between set-point and process variable), and  $K_p$ ,  $K_i$ , and  $K_d$  are proportional, integral, and derivative gains, respectively. Various factors including stability, fast response, small overshoot, and small steady-state error can affect the quality of the PID controller. In turn, selecting the optimal parameters (i.e.,  $K_p$ ,  $K_i$ , and  $K_d$ ) for the PID controller can be a pivotal process to determine these factors. For the current simulations, manual-tuning was employed to identify the optimal values of  $K_p$ ,  $K_i$ , and  $K_d$  by conducting simple iterative calculations [28].

A first-order thermal-chemical rate equation (called Arrhenius equation) was used to describe the degree of thermal damage in tissue for a period of time. The equation characterizes the rate when molecules become thermally denatured [17]. A dimensionless factor ( $\Omega$ ) was implemented to define irreversible thermal injury, which exponentially depends on temperature and irradiation time as follows:

$$\Omega(r, t) = A_f \cdot \int_0^\tau \exp\left(\frac{-E_a}{R \cdot T(r, t)}\right) dt \quad (9)$$

where  $A_f$  ( $1/s$ ) is the frequency factor,  $E_a$  ( $J/mol$ ) the denaturation activation energy,  $R$  ( $J/mol \cdot K$ ) the universal gas constant of  $8.314$ ,  $T$  ( $K$ ) the absolute temperature in tissue, and  $\tau$  ( $s$ ) the irradiation time.  $\Omega = 1$  indicates that 63% of tissue experiences the irreversible thermal

damage as the temperature rises from approximately 333 K [17]. Volume of the thermal damage in the tissue was also calculated for quantitative comparison with experimental results. Both undamaged ( $f_u$ ) and damaged ( $f_d$ ) fractions of the tissue were also described as  $f_u = \exp(-\Omega)$  and  $f_d = 1 - f_u$  to represent thermal damage index, respectively [24]. Table 2 summarizes all the thermal damage parameters used for the numerical simulations.

With optical and thermal properties known [13], liver tissue was used for numerical computation. As a near infrared wavelength of 980 nm was applied for the current study, optical scattering was considered significant during irradiation [29]. Thus, instead of  $\mu_a$ , the effective attenuation coefficient ( $\mu_{eff}$ ) was utilized, based upon diffusion approximation [25].

$$\mu_{eff} = \sqrt{3\mu_a \cdot [\mu_a + \mu_s \cdot (1-g)]} \quad (10)$$

where  $g$  is the anisotropy factor, and  $\mu_a$  was replaced by  $\mu_{eff}$  in Eq. (6) and 7. Typically, optical properties of soft tissue have a significant dependence on temperature as well as thermal damage index. Accordingly, dynamic variations in the optical properties of the liver tissue were considered as follows [24, 30, 31]:

$$\mu_a = \mu_{a,native} f_u + \mu_{a,coagulative} f_d \quad (11)$$

$$\mu_s = \mu_{s,native} f_u + \mu_{s,coagulative} f_d \quad (12)$$

$$g = g_{native} f_u + g_{coagulative} f_d \quad (13)$$

where  $\mu_{a,native}$  ( $cm^{-1}$ ),  $\mu_{s,native}$  ( $cm^{-1}$ ), and  $g_{native}$  are absorption coefficient, scattering coefficient, and anisotropic factor of the native tissue (i.e., undamaged tissue), respectively, and  $\mu_{a,coagulated}$  ( $cm^{-1}$ ),  $\mu_{s,coagulated}$  ( $cm^{-1}$ ), and  $g_{coagulated}$  absorption coefficient, scattering coefficient, and anisotropic coefficient of the coagulated tissue (i.e., thermally denatured tissue). Then,  $\mu_a$ ,  $\mu_s$ , and  $g$  in Eq. (10) were replaced by the ones in Eq. (11), 12, and 13. Table 2 lists the optical properties of the coagulated and native tissues.

**Table 2. Physical parameters of liver tissue used for thermal damage model**

Parameter	Native tissue	Coagulated tissue	Reference
Absorption coefficient ( $\mu_a$ , $cm^{-1}$ )	$0.64 \pm 0.02$	$0.41 \pm 0.02$	[31]
Scattering coefficient ( $\mu_s$ , $cm^{-1}$ )	$47.2 \pm 2.1$	$329.6 \pm 39$	[31]
Anisotropy factor	$0.93 \pm 0.003$	$0.91 \pm 0.02$	[31]
Frequency factor ( $A_f$ , 1/s)		$5.5 \times 10^{41}$	[15]
Activation energy ( $E_a$ , J/mol)		$2.77 \times 10^5$	[15]
Universal gas constant ( $R$ , J/mol·K)		8.314	[15]

The current model assumed that thermal properties of glass and air were constant during laser irradiation (Table 1). However, the thermal properties ( $\rho$ ,  $c$ , and  $k$ ) of liver tissue were considered variable on account of high water content in the tissue as well as dynamic changes in the thermal properties of water in the range of 20~100 °C [24, 32]:

$$\rho(T) = 1000 \cdot (1.3 - 0.3k_p \cdot w) \quad (14)$$

$$c(T) = 4190 \cdot (0.4 + 0.6k_c \cdot w) \quad (15)$$

$$k(T) = 0.4 \cdot (0.1 + 1.4k_k \cdot w) \quad (16)$$

where  $w$  is water mass percentage in the tissue (approximately 69% for liver tissue [30]). In addition,  $k_p$ ,  $k_c$ , and  $k_k$  are temperature-dependent factors for  $\rho$ ,  $c$ , and  $k$  of water and can be expressed as follows [24]:

$$k_p = 1 - 4.98 \times 10^{-4} \cdot (T - 20) \quad (17)$$

$$k_c = 1 + 1.02 \times 10^{-4} \cdot (T - 20) \quad (18)$$

$$k_k = 1 + 1.78 \times 10^{-3} \cdot (T - 20) \quad (19)$$

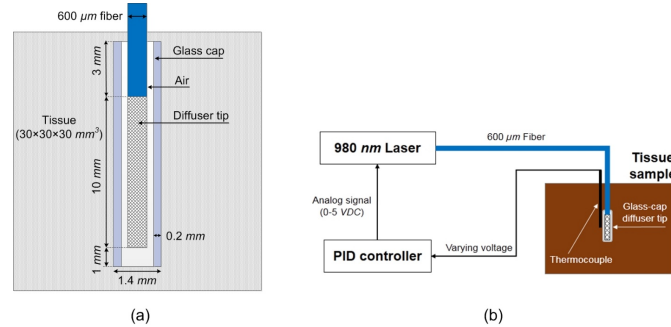


Fig. 2. Schematic illustrations on (a) geometry for numerical simulations and (b) experimental set-up for tissue testing under CW, pulsed, and PID-controlled modes

### 2.3. Experimental study

*Ex vivo* experiments were conducted to verify computational models in light of temperature elevation and degree of thermal denaturation. Figure 2(b) presents an experimental set-up for diffuser-assisted tissue coagulation. Similar to the numerical model, porcine liver tissue was selected as a sample for the *ex vivo* testing. The tissue was harvested from a local slaughter house and stored in isotonic saline at 4°C to prevent any dehydration and structural deformation. Each tissue specimen was prepared in size of 30×30×30 mm<sup>3</sup>. Prior to the testing, a 15-mm long cylindrical hole (1.4 mm in diameter) was drilled inside the tissue. Then, the diffusing applicator was inserted into the hole, and laser light was delivered to the liver tissue in an interstitial and circumferential manner. The initial temperature of the tissue was maintained at 20°C.

As a light source, a 10-W 980-nm laser system (Apollo Instrument, Irvine, California, USA) was employed for 30-s laser irradiation (i.e.,  $P_0 = 10$  W). The average irradiance on the tissue surface was estimated to be approximately 21.6 W/cm<sup>2</sup> for both simulations and experiments. To evaluate the real-time thermal response of the tissue (accuracy of ± 1.2°C) during the irradiation, a K-type thermocouple (TSL-101, Guageworld, Anyang, Korea) was interstitially placed parallel to the diffuser and positioned in the middle of the diffuser as presented in Fig. 2(b). A 0.5-mm thin white plastic plate was located between the diffuser and the thermocouple to prevent any direct light interaction along with self-heating. As aforementioned in the numerical section, three different modes were experimentally tested: CW, pulsed (pulse duration = 0.5 s and 50% duty cycle), and PID-controlled. For the PID application, the maximum temperature at the cap-tissue interface was maintained at 353 K to consistently entail irreversible thermal coagulation in the tissue. An industrial high accuracy PID controller (TK4 series, Autonics Corp., Busan, Korea) was utilized to measure the feedback temperature during the irradiation and connected to the laser system that was in an external mode. As a programmed function in the PID controller, auto-tuning was implemented to identify the optimal values for  $K_p$ ,  $K_i$ , and  $K_d$  during the tests. In principle, the auto-tuning can measure thermal characteristics and response rate in a subject and then calculate the PID parameters automatically in order to achieve fast response and high stability for the optimal temperature control [28]. Thus, the temperature feedback from the controller continuously modulated the laser power to maintain the identical temperature of 353 K in the tissue during the 30-s irradiation. It should be noted that the comparison between simulations

and experiments was based upon the single-point measurements as only one thermocouple was applied to examine temperature elevations.

To assess the development of thermal damage, the extent of irreversible tissue coagulation was quantified at various irradiation times ranging from 100 to 600 *s* with an increment of 100 *s*. Upon irradiation tests, each specimen was cross-sectioned along the axis of a diffusing applicator, and each cross-section was imaged by using a portable microscope. Image J (National Institute of the Health, Bethesda, MD) was used to measure physical dimensions (thickness and area) of each coagulated tissue. Coagulated regions were defined as discolored (i.e., tan color) areas in the tissue after the laser irradiation. Assuming that the shape of thermal coagulation is elliptical, the volume of each thermally denatured tissue was estimated by using the following equation [33];

$$V = \frac{4\pi}{3} \cdot \frac{x}{2} \cdot \frac{y}{2} \cdot \frac{z}{2} \quad (20)$$

where *x*, *y*, and *z* were the measured thicknesses of each coagulated tissue along *x*-, *y*-, and *z*-axis, respectively. Thus, the coagulation volumes were quantified at various irradiation times ranging from 100 *s* to 600 *s* with an increment of 100 *s* and compared between the simulations and the experiments. Each condition was performed five times (*N* = 5). Student's *t*-test was performed for statistical comparison and *p* < 0.05 means significant.

### 3. Results

Figure 3 shows spatial distributions of temperature (upper row) and thermal coagulation (lower row) from numerical simulations for CW (Fig. 3(a)), pulsed (Fig. 3(b)), and PID-controlled modes (Fig. 3(c)) after 30-s irradiation at 10 *W*. In general, the developments of both the temperature and the coagulation seemed pear-shaped along the diffuser irrespective of mode. For CW application in Fig. 3(a), the temperature at the diffusing tip increased up to 390 *K*, which was higher than the onset temperature for tissue carbonization (i.e. 373 *K* described as gray contour). The wide distribution of the thermal coagulation occurred around the diffuser, clearly reflecting the temperature distribution. Both the pulsed and the PID controlled modes yielded almost comparable distribution of the temperature as shown in Figs. 3(b) and 3(c), and the overall temperature was below 373 *K*. However, the extent of the thermal coagulation for the PID-controlled case was quite larger than that for the pulsed one. The coagulation region was principally developed near the proximal end of the diffuser (i.e. 2.5 *mm*), corresponding to the distribution of longitudinal emissions in Fig. 1(c).

Figure 4(a) presents a cross-sectional view of the temperature distribution at *z* = 6.5 *mm* along the diffusing applicator after 100-s irradiation at 10 *W* in a PID-controlled mode. Apparently, circular heat conduction occurred symmetrically around the diffuser axis, indicative of distribution of polar emissions in Fig. 1(b). A gray contour represents an isothermal region at 333 *K* (i.e. threshold temperature for tissue coagulation). Figure 4(b) exhibits temporal developments of the temperature at various radial distances (*r* = 0.7, 3, and 6 *mm*) from the diffuser axis during PID-controlled application (irradiation time = 100 *s*). The radial distance of 0.7 *mm* represents the interface between tissue and the glass-cap. Due to the PID-controlled mode, the temperature at the interface was initially maintained at 353 *K* as the pre-determined temperature (i.e., plateau in blue line) for 100 *s*, and the steady state error of the temperature was less than 0.5 *K*. After the irradiation, the temperature dropped exponentially with the time. On the other hand, as the radial distance increased (i.e., further away from diffuser axis), the temperature elevation rate was relatively slower and the plateau for the temperature saturation started to disappear. The lower maximum temperature was also achieved at the end of the irradiation with the increasing distances.

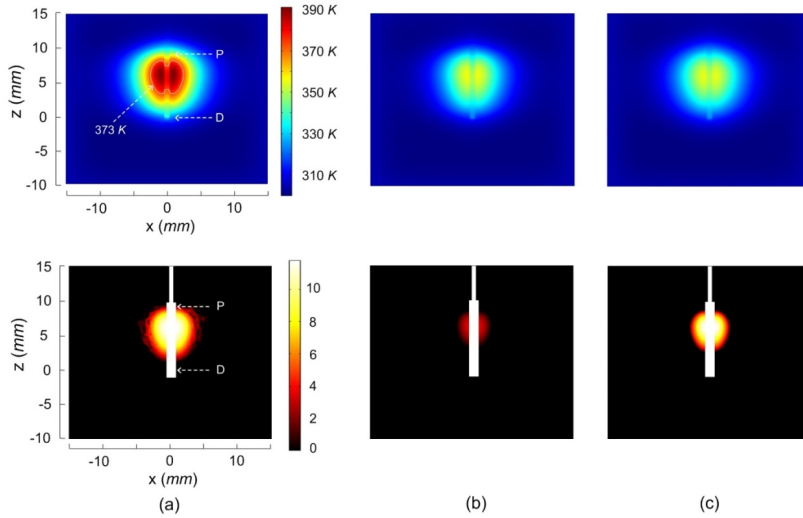


Fig. 3. Numerical analysis on spatial temperature distribution (top) and thermal coagulation (bottom) after 30-s irradiation at 10 W: (a) CW, (b) pulsed, and (c) PID-controlled modes. Note that a gray contour represents 373 K temperature for carbonization threshold. (P = proximal and D = distal ends)

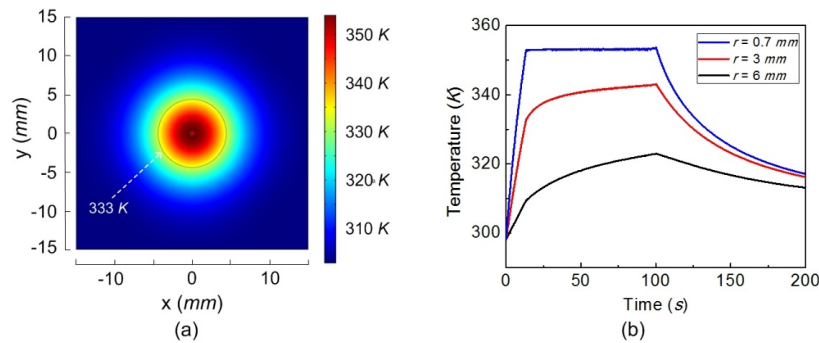


Fig. 4. Simulated temperature distribution for PID-controlled application at 10 W: (a) cross-sectional view of temperature at  $z = 6.5$  mm from proximal end of diffuser after 100-s irradiation and (b) temporal development of temperature at various radial distance (0.7, 3, and 6 mm) from axis of diffuser (irradiation time = 100 s).

Figure 5(a) demonstrates simulation results of temperature developments as a function of time under various modes at 10 W. Laser irradiation times for CW and pulsed modes were 30 s whereas a PID-controlled mode irradiated for a longer period of 100 s to validate the steady-state temperature level of 353 K. The temperature was measured at the tissue-glass cap interface (i.e.  $r = 0.7$  mm in Fig. 4), and the initial temperature was 293 K. In the CW mode, the temperature rapidly increased at the average rate of 3.2 K/s and reached the maximum value of 391 K at the end of light exposure. After laser power was off, the temperature exponentially decreased at the average rate of 0.5 K/s. The temperature reached 353 K (pre-determined temperature for PID-controlled mode) in 15 s. The pulsed mode exhibited a 30% lower thermal gradient of 2.0 K/s during the irradiation and reached the 10% lower maximum temperature of 354 K in 30 s, in comparison with the CW mode. Then, the temperature rapidly decreased with time at the average rate of 0.3 K/s. The pulsed mode attained the temperature of 353 K in 29 s, which was almost two-fold longer than that of the CW mode. The PID-controlled mode initially entailed a thermal gradient of 0.4 K/s. Upon reaching 353 K in 15 s, the temperature was invariably maintained at the same temperature until the laser was off at 100 s and then decreased at the average rate of 0.4 K/s. It was noted that both the

CW and the PID-controlled modes showed a comparable temperature increase rate for the first 15-s irradiation. Figure 5(b) presents experimental results of temperature elevations under the CW, pulsed, and PID-controlled modes at 10 W. The CW mode induced the 14% higher maximum temperature of 408 K (i.e., temperature difference = 17 K) with a 20% faster increase rate of 3.8 K/s, compare with the simulation results in Fig. 5(a). After the irradiation was terminated, the temperature exponentially decreased at the average rate of 0.6 K/s. The temperature reached 353 K in 10 s, indicative of 33% more rapid development than the simulations. After the CW application, partial carbonization was vividly observed on the tissue surface as the simulation predicted in Fig. 3(a). In the case of the pulsed mode, the temperature was developed at the average rate of 2.0 K/s, and the maximum temperature reached 354 K in 30 s. Then the temperature began to decrease (thermal gradient = -0.3 K/s). On the other hand, the PID-controlled application initially increased the temperature up to 353 K in almost 12 s and maintained the constant temperature for the rest of the exposure time. Upon termination of irradiation, the temperature dropped at the average rate of 0.4 K/s. No carbonization was observed for both the pulsed and PID-controlled modes. It should be noted that the overall temperature behaviors for all the modes were almost equivalent between the numerical simulations and the experiments (Figs. 5(a) and 5(b)).

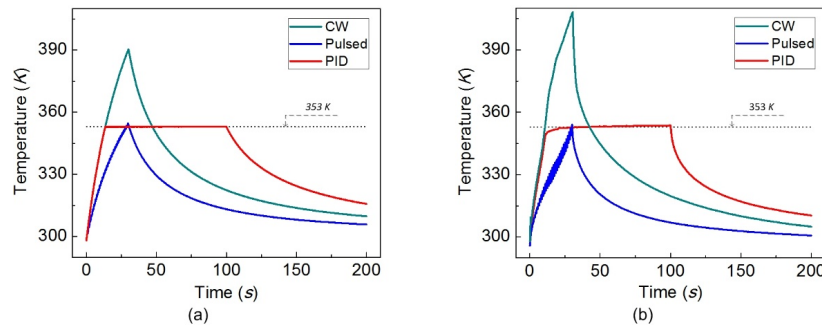


Fig. 5. Temporal developments of temperature at tissue-glass cap interface for CW, pulsed, and PID controlled applications during and after 10-W laser irradiation (irradiation times = 30 s for CW and pulsed and 100 s for PID-controlled): (a) numerical simulations and (b) experiments. Note that the PID-controlled temperature was set at 353 K during the irradiation.

Figure 6 compares power modulation controlled by PID algorithms between numerical simulations (Fig. 6(a)) and experiments (Fig. 6(b)) during photocoagulation in a PID-controlled mode. A PID controller was employed to constantly regulate the amount of laser power (i.e. initial input power = 10 W) to maintain the pre-determined temperature of (353 K) at the tissue-glass interface and thus to achieve consistent tissue coagulation during the irradiation. According to the numerical simulations in Fig. 6(a), the modulated power was firstly maintained at 10 W for 15 s, indicating that the constant power continued to increase the temperature from 293 K (initial temperature) to 353 K (pre-determined temperature). Then, the power suddenly dropped from 10 W to around 2 W in 2 s and began to fluctuate between 2 and 4 W for around 10 s to reduce the amount of laser energy delivery to the tissue. At 30 s, the power abruptly decreased further down to 0 W and increased again to 2 W at 45 s. A period of the transient state was estimated to be 30 s (= 45 s - 15 s). Afterward, the power went into the steady-state and started to fluctuate between 0.2 and 3 W to sustain the thermal equilibrium at the tissue-glass cap interface (i.e., 353 K). The experiments in Fig. 6(b) presented a similar tendency in the overall power modulation. However, the constant power of 10 W was initially applied to the tissue for 10 s and then decreased and began to fluctuate between 0 and 3 W at 25 s, which represented the onset of the steady-state. It was noted that the transient state for the experiments (13 s = 25 s - 12 s) was 57% shorter than that for the numerical simulations (30 s). The faster response of the PID controller in the experiments indirectly reflected significant increase in temperature as shown in Fig. 5(b).

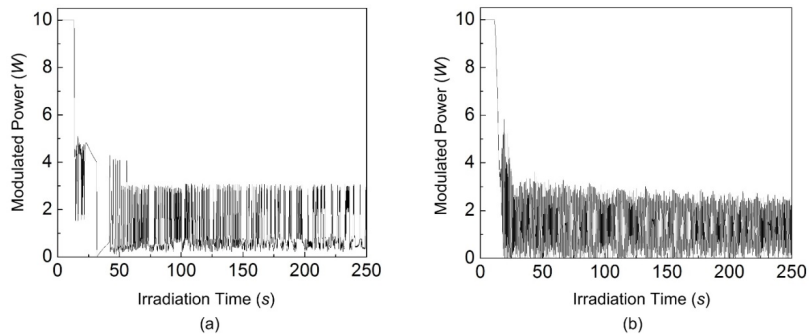


Fig. 6. Comparison of power modulation during 10- $W$  laser irradiation for 250  $s$ : (a) numerical simulations and (b) experiments

Figure 7 exhibits developments of irreversible thermal denaturation at various irradiation times (100, 300, and 600  $s$ ) in a PID-controlled mode at 10  $W$ . The upper images represent numerical simulations whereas the bottom images experiments. In the theoretical results, black background is soft tissue whereas the colored area means the denatured tissue. The dotted lines in the experimental results indicate the boundary of the irreversibly coagulated tissue (i.e., discolored region). Regardless of the irradiation time, both the numerical simulations and the experiments yielded almost comparable tissue coagulation. The extent of the thermal denaturation seemed ellipsoidal and gradually expanded with the irradiation time for both the cases. After 600  $s$ , the tissue coagulation circumferentially covered the entire length of a diffusing tip as presented in Fig. 7(c). It was noted that the coagulated area was slightly skew to the right (distal end of diffuser), corresponding to the spatial distribution of longitudinal emissions in Fig. 1(c). According to the experiments, the irradiation time of 600  $s$  generated a coagulation area of 95  $mm^2$  in tissue, which was 90% and 34% larger than 100  $s$  (50  $mm^2$ ) and 300  $s$  (71  $mm^2$ ), respectively. Volumetric thermal coagulation was quantitatively compared as a function of irradiation time (from 100  $s$  to 600  $s$  with increment of 100  $s$ ) between the numerical simulations and the experiments in Fig. 8. The dotted lines represent a linear fitting. Overall, both the simulations and the experiments presented that the coagulation volume increased linearly with the irradiation time ( $R^2 = 0.96$  for simulations vs. 0.99 for experiments). However, the volumes from the experiments were slightly (0~10%) larger than those of the simulations. At longer irradiation times (400  $s$  or longer), the volumetric differences began to gradually increase between the simulations and the experiments. The irradiation time of 600  $s$  promoted the coagulation volume ( $1.04 \pm 0.02 \text{ cm}^3$  for experiment) by three-fold, compared with that of 100  $s$  ( $0.36 \pm 0.01 \text{ cm}^3$  for experiment) for both the cases. It should be noted that the simulations matched well with the experimental phenomena in terms of thermal denaturation volume.

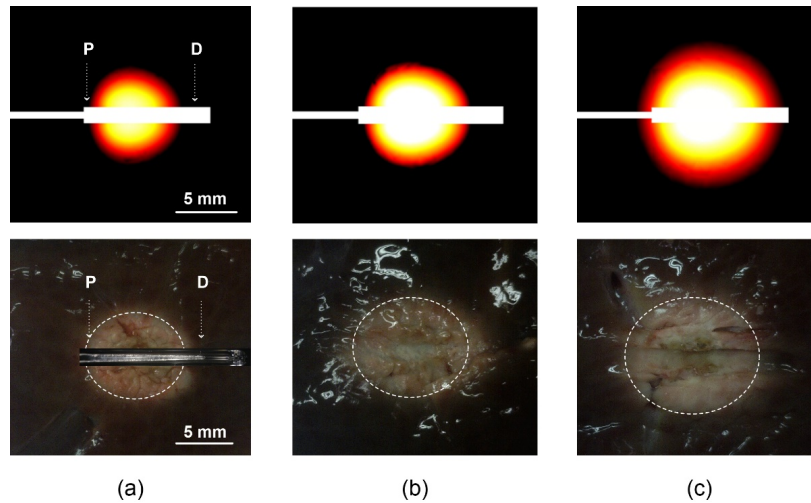


Fig. 7. Comparison of thermal denaturation regions between theoretical and experimental results with PID-controlled application after irradiation times of (a) 100 s, (b) 300 s, and (c) 600 s at 10 W (P = proximal and D = distal ends)

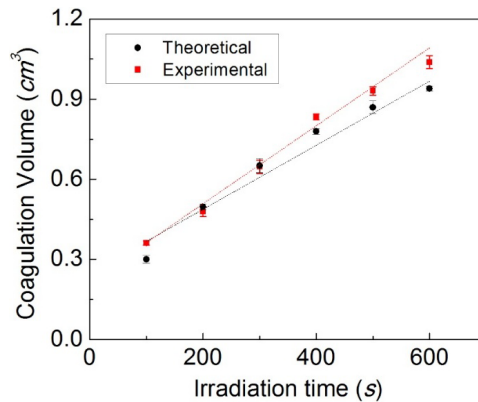


Fig. 8. Quantification on coagulation volume as function of irradiation time for numerical simulations and experiments under 10-W irradiation with PID-controlled application.

#### 4. Discussion

The aim of the current study was to theoretically and experimentally investigate the feasible application of a temperature feedback-controller during diffuser-assisted photothermal treatment on pancreatic tumors. Both numerical simulations and experiments validated the functions of the PID-controller that constantly maintained tissue surface temperature and thus achieved consistent tissue coagulation (Figs. 5 and 8). Uniform circumferential emissions from the diffusing applicator (Fig. 1(b)) vividly resulted in radial temperature distribution around the diffuser axis in the simulations (Fig. 4(a)), which well agrees with the previous experiment [15]. The left-skewed longitudinal emissions in Fig. 1(c) entailed slightly asymmetric development of the temperature and the thermal coagulation along the diffuser in both the simulations (Fig. 3) and the experiments (Fig. 7). The PID-controlled application attained the pre-determined temperature (353 K) for tissue coagulation theoretically and experimentally. Then, the temperature was invariably maintained during laser irradiation (Figs. 4 and 5) due to constant power modulations (Fig. 6). According to the numerical modeling and the experiments, the constant surface temperature linearly promoted the degree of the tissue coagulation with irradiation time without carbonization, implicating the reliable

estimate on treatment margins (Fig. 8). Therefore, the proposed PID-controlled laser treatment can be a feasible therapeutic modality to treat pancreatic tumors in a safe and effective manner.

To identify the optimal conditions for photothermal treatments, three different irradiation modes (CW, pulsed, and PID-controlled) were compared numerically and experimentally. In the case of the CW mode, the temperature within the tissue was rapidly elevated due to constant supply of optical energy, leading to unwanted thermal injury (carbonization) at the tissue surface during the treatment (Figs. 3(a) and 5). The pulsed mode involved relatively slow temperature development, which resulted from less energy delivery (i.e., 50% duty cycle) as well as periodic cooling from the repetitive pulses (Fig. 5). Accordingly, in spite of reaching the coagulation threshold (353 K), the extent of the tissue coagulation was quite limited, in comparison with the CW and the PID-controlled modes (Fig. 3(b)). On the other hand, the PID-controlled mode initially obtained as rapid temperature elevation as the CW mode and later sustained the constant temperature of 353 K on account of the temperature feedback (Fig. 5). As a result, the irreversible tissue denaturation was gradually promoted without any surface carbonization (Figs. 3(c) and 7). Hence, the PID-controlled application demonstrated a feasible way to achieve consistent tissue coagulation along with minimal thermal injury at the surface.

Typically, the quality of a PID controller depends on the design and tuning methods of PID algorithms. According to the current study, manual-tuning was implemented for numerical simulations whereas auto-tuning for experiments. The manual-tuning method is simple but requires experienced operations [28]. In order to prevent the overshoot temperature during the transient state as well as to minimize the steady-state errors, the parameters for the PID controller (i.e.,  $K_p$ ,  $K_i$ , and  $K_d$ ) were carefully calculated by means of iterations. In turn, the PID factors were selected to be 15 1/K for  $K_p$ , 0 for  $K_i$ , and 0.1 s/K for  $K_d$  to achieve the critically-damped response. On the other hand, for the experiments, the auto-tuning method was based upon a built-in algorithm executed by a microprocessor in the controller, which constantly determined the optimal values for the PID factors during the tests. Both the theoretical and the experimental studies in Figs. 5 and 6 demonstrated that the temperature responses were critically-damped in spite of different tuning methods. Thus, almost no overshoot temperature (i.e., less than 0.5 K) was found during the transient state, eventually preventing any tissue vaporization or carbonization. Moreover, the steady-state errors for both the cases were less than 1 K. Therefore, it was confirmed that the PID controllers employed for the simulations and the experiments showed a good agreement by maintaining the desired temperature of 353 K in the tissue.

Although numerical simulations generally reflected experimental results, there were still slight discrepancies in light of thermal response. According to Fig. 5, a CW mode showed that the peak temperature from the experiments was 14% higher than that from the simulations (temperature difference = 17 K). The experiments also reached the pre-determined temperature (353 K) 33% faster during the CW mode, in comparison with the simulations (15 s for simulation vs. 10 s for experiment). The different thermal behaviors for the CW mode can be explained by surface carbonization (Figs. 3 and 5(b)). Conceivably, the formation of the tissue carbonization during the experiments could immediately augment light absorption characteristics, significantly promoting the temperature rise in the tissue [17]. Although both optical and thermal properties were considered to be inconstant during the simulations (Eq. (11)-19), the dynamic variations in tissue properties merely reflected the native and denatured tissue conditions. Thus, abrupt property changes in association with the carbonization could account for faster and higher elevations in the temperature for the CW mode. For a PID-controlled mode, the experiment yielded a 20% shorter response time (12 s) to reach the steady state (i.e., constant temperature of 353 K) than the simulations did (15 s), which also reflected a 57% shorter response time in power modulations in Fig. 6 (30 s for simulations vs. 13 s for experiments). The slight discrepancy might pertain to less accurate

expressions of the dynamic variations in the tissue properties. In fact, the tissues properties used for the current simulations were based upon liver tissue owing to lack of pancreas data. Furthermore, as a diffuser was interstitially placed in the tissue (i.e., close volume), the integrating sphere effect during heat deposition could contribute to the enhanced optical interactions with the targeted tissue due to multiple scattering effects at the tissue-glass cap interface [34]. Hence, in order to further enhance computational analysis, Monte Carlo simulation with time-dependent optical properties will be incorporated with the thermal models to track spatial photon distribution in the tissue. Convective heat loss due to blood perfusion should be also reflected to predict thermal responses during and after the photocoagulation. Optical and thermal properties for pancreatic tissue should also be measured to enhance the accuracy of numerical modeling. In spite of the slight inconsistencies, the developed computational modeling could be a feasible analytic tool to estimate thermal behaviors of the targeted tissue during the PID-controlled laser treatment and eventually to identify the optimal therapeutic parameters for the maximum clinical outcomes.

According to the Arrhenius equation, thermal damage volume is mainly a function of local temperature in tissue and exposure time. Since the current study constantly limited the surface temperature at 353 K during the PID application, the extent of the thermal damage in the tissue was principally dependent on the irradiation time (Fig. 8). Thus, both numerical and experimental results demonstrated a linear relationship between coagulation volume and the irradiation time in Fig. 8. However, the volumetric differences (0~10%) between the two cases occurred possibly due to variations in thermal sensitivity from empirical values of  $A_f$  and  $E_a$ . Due to lack of data availability, the current model simply used constant values for the damage parameters, which should be temperature-dependent. Additionally, as the coagulation volume increased with the irradiation time, the margin of each coagulated area was rather unclear, possibly leading to measurement errors (i.e., overestimation).

To translate the current research into practical applications, further investigations on PID-controlled photothermal treatments still remain. For the sake of experimental reliability, the tip of a thermocouple was positioned in the middle of the diffuser to measure the real-time temperature. However, due to asymmetric (left-skewed) light distribution in Fig. 1(c), the measured temperature might be contingent upon the position of the thermocouple. In fact, to ensure safety of the proposed treatment, the temperature should be assessed at various positions of the diffusers to define the range of the temperature fluctuations from the proximal (maximum temperature) to the distal end (minimum temperature). Instead of the thermocouple, a non-invasive photoacoustic technique can also be integrated with the proposed photothermal treatment to measure the interstitial tissue temperature. Currently, to achieve more even light distribution such as flat-top profile, various fabrication patterns are being implemented to the diffuser tip, which can accompany more predictable thermal behaviors and uniform generation of tissue coagulation. A number of wavelengths should be evaluated to confirm the versatility of the PID-controlled photothermal treatment in light of thermal penetration depth as well as temperature increase. Furthermore, *in vivo* preclinical studies with tumor-injected mini pigs should be performed to assess the effect of blood perfusion on the temperature development, to validate the degree of thermal coagulation for optimizing therapeutic parameters, and to identify acute and chronic responses of the treated tissue as well as tissue healing associated with collagenous fibrosis.

## 5. Conclusion

A theoretical and experimental analysis demonstrated the feasibility of temperature feedback-controlled photothermal treatment for pancreatic coagulation. Circumferential light emissions can achieve uniform coagulation in a tubular tissue structure. The current numerical model can be a useful analytical tool to describe the interstitial thermal effects as well as to determine the optimal therapeutic conditions. Both constant surface temperature and linearly

increasing coagulation volume can regulate the extent of the treatment regions during laser irradiation. Further *in vivo* studies will be performed to validate the current technique and to identify acute and chronic tissue responses with healing process. The proposed PID-controlled photothermal treatment with a diffusing applicator can be a therapeutic modality to treat pancreatic tumors by maintaining constant surface temperature in a circumferential manner.

### **Acknowledgments**

This research was supported by a grant from Marine Biotechnology Program (20150220) funded by Ministry of Oceans and Fisheries, Korea. Trung Hau Nguyen and Suhyun Park equally contributed to this work.